Ultrastrong Capacitive Coupling of Flux Qubits

María Hita-Pérez, Gabriel Jaumà, Manuel Pino,[*,†] and Juan José García-Ripoll
Institute of Fundamental Physics IFF-CSIC, Calle Serrano 113b, Madrid 28006, Spain

(Received 6 August 2021; revised 28 September 2021; accepted 9 December 2021; published 24 January 2022)

A flux qubit can interact strongly when it is capacitively coupled to other circuit elements. This interaction can be separated into two parts, one acting on the qubit subspaces and one in which excited states mediate the interaction. The first term dominates the interaction between the flux qubit and an LC resonator, leading to ultrastrong couplings of the form $\sigma^y(a+a^\dagger)$, which complement the inductive $\sigma^x i(a^\dagger - a)$ coupling. However, when coupling two flux qubits capacitively, all terms need to be taken into account, leading to complex nonstoquastic ultrastrong interaction of types $\sigma_1^y\sigma_2^y$, $\sigma_1^z\sigma_2^z$, and $\sigma_1^x\sigma_2^x$. Our theory explains all these interactions, describing them in terms of general circuit properties—coupling capacitances, qubit gaps, inductive, Josephson and capacitive energies—that apply to a wide variety of circuits and flux qubit designs.

DOI: 10.1103/PhysRevApplied.17.014028

I. INTRODUCTION

Flux qubits are superconducting loops with one or several Josephson junctions that, when the qubit is threaded by a magnetic flux, create a frustrated inductive energy landscape. The qubit's low-energy space is built from quantum superpositions of persistent current states with opposite directions [1–4]. Flux qubits exhibit strong magnetic interactions and large anharmonicities while retaining good coherence times [5–9]. These are useful properties to implement fast qubit gates [10,11], perform quantum annealing [12–16], or to simulate strongly coupled quantum systems [17–27].

A flux qubit is usually described by two observables: the tunneling between persistent current states σ^z, and the qubit's magnetic dipole moment σ^x. The former accounts for the energy splitting Δ between current superpositions due to tunneling at the symmetry point $H = \Delta\sigma^z/2$ [2]. The dipole moment appears in the inductive coupling to microwave photons $g\sigma^x(a^\dagger + a)$ and to other flux qubits $J_{xx}\sigma_1^x\sigma_2^x$. An open question is how to escape the narrow framework provided by these interactions, allowing flux qubits to simulate nonstoquastic Hamiltonians, those that exhibit a sign problem when solving them via quantum Monte Carlo [28–32] and that enable universal adiabatic quantum computation [33–37].

There is still no completely satisfactory framework to implement different flux qubit couplings. One may obtain a ZZ interaction by converting the main qubit junction into a superconducting quantum interference device (SQUID), and coupling those SQUIDs to each other inductively [1]. However, the resulting interaction is weak and decreases monotonically with the gap, making it unsuitable for general quantum simulation and quantum annealing [38]. A similar coupling for qubits displaying nontrivial topological effects [39–41] could give the desired interaction [38], but those qubits may suffer from an enhanced susceptibility to charge noise [1,42]. The most promising approach so far is the capacitive coupling between flux qubits. Experiments with flux qubits [32,43] have demonstrated capacitive interactions along more than one direction [44], but the coupling strength seems to be limited and there is no analytical framework to understand the range of available interactions.

In this work we introduce an analytical model for the capacitive coupling of flux qubits to other superconducting circuit elements (cf. Fig. 1), complemented by a nonperturbative numerical treatment. We obtain the shape and scaling of the interaction between a qubit and a microwave resonator, and also between two flux qubits. We provide evidence of ultrastrong qubit-resonator interaction mediated by the electric dipole moment σ^y, thereby extending the family of ultrastrong inductive couplings [17,18,23], which are mediated by σ^x terms. For two capacitively coupled qubits, we explain the appearance of complex interactions along multiple directions, YY, ZZ, and XX. This is a rich landscape of spin Hamiltonians for quantum simulation, quantum annealing, and quantum computation, which exceeds the simple picture from spectroscopic characterizations [32] and complements earlier numerical studies [44] with scalings based on a qubit's design parameters and a modelization of interactions mediated by excited states.

[*]manuelpino@usal.es
[†]Present address: Nanotechnology Group, USAL-Nanolab, Universidad de Salamanca, E-37008 Salamanca, Spain.

 © 2022 American Physical Society

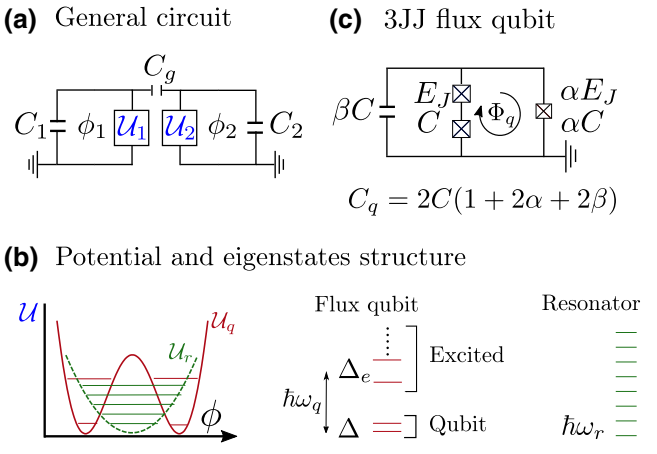

FIG. 1. (a) Two superconducting circuits, described by flux variables ϕ_i, coupled by a capacitance C_g. (b) The first circuit is a flux qubit and the second is either an identical qubit or an LC resonator. The flux qubit, operated at full frustration, is described by an inductive potential $\mathcal{U}_q$ with two identical wells (solid line). The relevant energy scales are the qubit Δ, the energy differences between states in the same well $\hbar\omega_q$ and, for deep potentials, the splitting Δ_e between excited states. The resonator has a quadratic potential $\mathcal{U}_r$ (dashed) and a harmonic spectrum with equispaced energies, separated by $\hbar\omega_r$. (c) Our simulations use three Josephson-junction flux qubits, with a central junction α times smaller, a possible shunting capacitance β, and a magnetic flux $\Phi \simeq \Phi_0/2$. The charging and Josephson energies of the large junctions are denoted by E_J and $E_C = e^2/(2C)$.

II. MODEL

We study on equal footing both the qubit-qubit and qubit-resonator capacitive couplings, as shown in Fig. 1. Each element, qubit or resonator, is represented by a flux ϕ and a charge q operator, and the type of circuit is determined by the inductive potential $\mathcal{U}$. The Hamiltonian $H = H^{(0)} + \epsilon V$ splits into bare circuits and an interaction, see Appendix A [45]:

$$H^{(0)} = \sum_{i=1,2} \frac{q_i^2}{2C_i} + \mathcal{U}_i(\phi_i), \tag{1}$$

$$V = -\frac{q_1 q_2}{\sqrt{C_1 C_2}} - \sqrt{\frac{C_2}{C_1}}\frac{q_1^2}{C_1} - \sqrt{\frac{C_1}{C_2}}\frac{q_2^2}{C_2}. \tag{2}$$

Here $C_{1,2}$ are the capacitances of bare circuits, C_g is the coupling capacitance, and $\overline{C}_{\rm OD} = \left[C_1C_2 + (C_1 + C_2)C_g\right]/C_g$ is the off diagonal of the inverse capacitance matrix. The strength of the coupling is controlled by $\epsilon = \sqrt{C_1C_2}/\overline{C}_{\rm OD}$, with $\epsilon \sim \mathcal{O}(C_g)$ for $C_g/C_{1,2} \ll 1$.

The first circuit is always a flux qubit $C_1 = C_q$. The second circuit will be either an identical qubit $C_2 = C_1$, or a microwave resonator $C_2 = C_r$. Without loss of generality, we study three Josephson-junction qubits (3JJQs) [cf. Fig. 1(c)], operating at full frustration, with half a flux quantum $\Phi_q = \Phi_0/2$ in the loop. In this situation, this or any other similar qubit will exhibit an inductive potential $\mathcal{U}_{1,2}$ with local minima at $\phi = \pm\varphi_\star(\Phi_0/2\pi)$. Each minima is associated with one persistent current state and a local excitation energy $\hbar\omega_q$. We present results in terms of the relative coupling $\gamma = C_g/C$ of the 3JJQ, where C is the large qubit junction of the 3JJQ. For the resonator, we use a quadratic inductive potential $\mathcal{U}_2 = \phi_2^2/(2L_r)$ with resonator frequency $\omega_r = 1/\sqrt{L_rC_r}$.

III. METHODS

We model the whole system as an effective qubit-resonator or qubit-qubit Hamiltonian, using a Schrieffer-Wolff transformation $U(\epsilon)$ [45] that maps the eigenspaces of H to the eigenspaces of the bare model $H^{(0)}$. In our analytical treatment, we start from a projector P_0 onto a low-energy subspace—e.g., the four-dimensional space of two qubits, or a tensor product of a qubit and resonator spaces—and develop the effective Hamiltonian as a perturbative series

$$H_{\rm eff} = P_0H^{(0)}P_0 + \sum_{n=1} \epsilon^n \mathcal{M}_n. \tag{3}$$

The first-order term is the projection of the interaction onto the qubit subspace $\mathcal{M}_1 = P_0^\dagger V P_0$, while the $\mathcal{M}_{i\geq 2}$ describe interactions mediated by virtual transitions, see Appendix B [45].

Numerically, we could imitate this procedure, but instead we sum the series to all orders, as $H_{\rm eff} = P_0UHU^\dagger P_0$, where U is the Schrieffer-Wolff transformation. The algorithm is based on computing numerically the transformation $UP = P_0U$ that maps the exact eigenstates of H to $H^{(0)}$, where P is the projector onto the low-energy sector of the coupled system. As explained in Ref. [44], this can be done by working on a truncated space of eigenstates, where $U = \sqrt{(1-P_0)(1-P)}$ is estimated. Alternatively, one may work with the lower-rank matrices UP and P_0U, as explained elsewhere [46]. Using this transformation, we compute the effective model $H_{\rm eff}$ and expand it on the basis of Pauli and Fock operators. This allows us to compare the effective Hamiltonian to the predictions from perturbation theory, validating the type and scaling of the coupling terms.

One needs to be careful when applying this theory to a composed system in which their low-energy sectors have very different energy scales. In this case, the low-energy dynamic of one of the systems may excite the other one outside of its low-energy subspace. For instance, when a resonator is very strongly driven and is in contact with the flux qubit, it may excite the qubit outside its low-energy subspace, invalidating the Schrieffer-Wolff approximation. In practice, this limitation is not very different from the experimental limitations that one faces when working with qubits in general superconducting experiments.

IV. THE COUPLING AT FIRST ORDER

The interaction V has two terms that renormalize the bare circuits, and only one that entangles their dynamics, $V_c = -q_1 q_2/\sqrt{C_1 C_2}$. To develop the first-order correction $\mathcal{M}_1$, we must express the charges q_i in the qubit and resonator basis. For the resonator, $q_2 = \sqrt{\hbar/2Z}(a^\dagger + a)$ exactly, in terms of Fock operators $\{a, a^\dagger\}$ and the resonator impedance $\mathcal{Z}$. For the flux qubit q_1, we assume that the renormalized Hamiltonian is anharmonic and that $H_1 \simeq \Delta\sigma_1^z/2$. We derive the voltage operator projected onto the qubit subspace $\mathcal{V}_1$ as the derivative of the flux $\mathcal{V}_1 \simeq i[H_1, \phi_1]/\hbar = (\Phi_0/2\pi)(\varphi_\star \Delta/\hbar)\sigma_1^y$, approximating the flux operator as the flux jump between qubit states $\phi_1 = (\Phi_0/2\pi)\varphi_\star \sigma^x$. Since $\mathcal{V}_1 = q_1/\overline{C}_1$ for the bare renormalized qubit, the projected charge operator is $q_1 \simeq \Phi_0 \overline{C}_1 \Delta \varphi_\star \sigma_1^y/h$.

Using this method, we obtain the first-order effective interaction between a qubit and a resonator $H_{qr}^{(1)} = g_{qr}^{(1)}\sigma_1^y(a^\dagger + a)$ with

$$\frac{g_{qr}^{(1)}}{\Delta} = \frac{\overline{C}_q}{\overline{C}_{\rm OD}}\frac{\varphi_\star}{2}\sqrt{\frac{1}{2\pi G_0 \mathcal{Z}}} \tag{4}$$

and the interaction between two qubits $H_{qq}^{(1)} = g_{qq}^{(1)}\sigma_1^y\sigma_2^y$ with

$$\frac{g_{qq}^{(1)}}{\Delta} = \frac{\overline{C}_q \varphi_\star^2}{\overline{C}_{\rm OD}}\frac{\Delta}{8E_C^q}. \tag{5}$$

Everything depends on the qubit's renormalized gap Δ, the resonator impedance $\mathcal{Z}$, the conductance quantum G_0, and the qubit's charging energy $E_C^q = e^2/(2\overline{C}_1)$.

This treatment neglects higher-order terms in the perturbation series (3), generated by matrix elements of the qubit's charge operator $(\mathbb{1} - P_0)q_1 P_0$ connecting qubit states with excited states delocalized among the inductive potential wells. Those elements grow as $q_1 \sim \sqrt{\omega_q}$, requiring us to analyze their effect on a case-by-case basis.

V. ULTRASTRONG QUBIT-RESONATOR COUPLING

Let us discuss the capacitive coupling of a flux qubit and an LC resonator. The second-order corrections to the capacitive coupling involve a simultaneous excitation of the qubit and the resonator, which acquire an energy $\hbar\omega_q$ due to leaving the qubit space and $\hbar\omega_r$ due to the creation or annihilation of a photon. While the amplitude of these processes in ϵV_c grows as $\hbar\sqrt{\omega_q\omega_r}$, the resonator cannot easily absorb the energy $\hbar\omega_q$. Thus, higher-order corrections $\mathcal{M}_{i\geq 2}$ only renormalize the qubit's self-energy and the capacitive coupling is fully captured by Eq. (4).

We confirm this hypothesis through a comparison with the full Schrieffer-Wolff numerical transformation for the full superconducting circuit of a 3JJQ [cf. Fig. 1(c)] coupled to a resonator. In terms of qubit and photon operators, it takes the form $H_{\rm eff} \simeq \Delta\sigma^z/2 + \hbar\omega a^\dagger a + g\sigma^y(a^\dagger + a)$ for moderate numbers of photons. As shown in Fig. 2(a), all the coupling constants from different designs of qubit and resonator collapse into the first-order correction derived analytically (4), up to coupling strengths $g/\Delta \approx 0.5$ beyond the perturbative limit. Since our model only demands a qubit anharmonic spectrum, we conclude that Eq. (4) is a general theory for the capacitive interaction between flux qubits and microwave resonators.

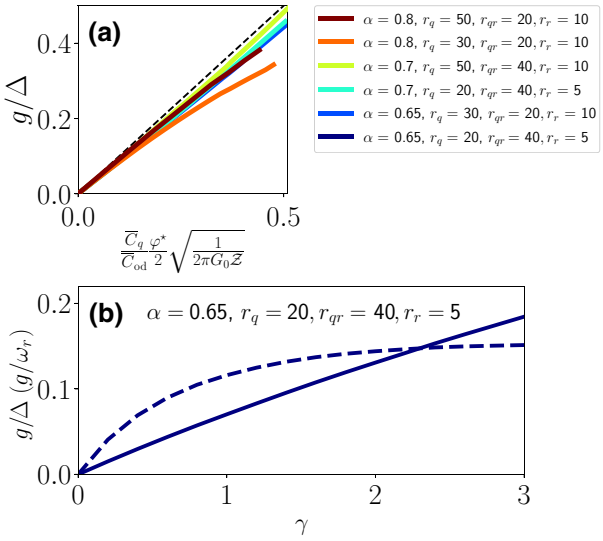

FIG. 2. A 3JJQ capacitively coupled to an LC resonator. (a) Coupling divided by qubit gap Δ as a function of the first-order corrections (the dashed line is the theoretical prediction for those corrections). We only show data for which higher corrections are negligible. The design parameters for all the panels are the qubit large junction energy ratio $r_q = E_J/E_C$, the energy ratio for the resonator $r_r = E_J^r/E_C^r$, and the ratio of resonator and qubit Josephson energies $r_{qr} = E_J/E_J^r$. The Josephson energy for the resonator as a function of its inductance L_r is $E_J^r = (1/L_r)(\hbar/2e)^2$. (b) Coupling divided by the qubit gap (solid line) and resonator energy (dashed) as a function of the ratio $\gamma = C_g/C$ between the shared capacitance and the qubit's large junction capacitance.

Unlike the inductive case [17,18,23], exploring the designs where ultrastrong coupling, $g/\omega_r \sim g/\Delta \geq 12\%$, occurs is complicated, because one has to consider the renormalization of the qubit's gap, while the resonator remains more or less unperturbed. After a careful analysis of the qubit parameter space, we have realized that this regime can be achieved for junctions with an intermediate ratio of $r = E_J/E_C \sim O(10)$, between those used in flux qubits $r \sim O(10^2)$ [3,8] and those used in fluxonium qubits $r \sim O(1)$ [47,48]. Still, we find a flux qubit with standard properties because the apparent increase in E_C is compensated by the increase of the qubit capacitance due to the coupling.

Using a 3JJQ with $r = 20$, we find evidence of an ultrastrong coupling regime with $g/\Delta \approx 0.15$ at zero detuning; see Fig. 2(b). This coupling is significantly larger than the flux qubit resonator capacitive couplings in previous works [49,50]. For the experimental realization of ultrastrong coupling, one can set the qubit large junction $E_J \approx 20$ GHz, a similar junction to those used in Table 2, device H, of Ref. [51]. This would give an ultrastrong coupled qubit-resonator system with a resonator frequency around $\omega_r = \sqrt{8E_J^r E_C^r} \approx 1$ GHz.

VI. QUBIT-QUBIT COUPLING

Let us now discuss the capacitive interaction between two flux qubits. We begin by presenting the numerically exact Schrieffer-Wolff transformation for two 3JJQs. In Fig. 3(a) we plot the interaction coefficients that result from expanding H_{eff} in the basis of Pauli matrices. The numerical model clearly shows the first-order terms associated with the σ^y charge dipole operator in Eq. (5). However, the flux qubits also acquire a comparable ZZ interaction that enables the tunneling of current states, and we also find a residual inductive XX. Note that, while the capacitive term induces a renormalization of the qubit's gap Δ, the qubit nature is preserved by an improvement in the qubit's relative anharmonicity α_r [cf. Fig. 3(b)]. Only at very large γ, the form of the interactions approaches $-g(\tilde{\sigma}_1^+\tilde{\sigma}_2^+ + \tilde{\sigma}_1^-\tilde{\sigma}_2^-)$, with ladder operators in the persistent current base $\tilde{\sigma}_i^{\pm} = \tilde{\sigma}_i^z \pm i\tilde{\sigma}_i^y$. In this limit, the coupling produces a large mass in the direction $\phi_1 - \phi_2$ of the two-qubit system and strongly suppresses transitions of the form $\tilde{\sigma}_1^+\tilde{\sigma}_2^- + \tilde{\sigma}_1^-\tilde{\sigma}_2^+$ [52]. In this limit, we obtain strongly interacting two-qubit systems with couplings larger than the qubit gap, around twice the value from previous works [44], and similar design parameters to other qubits that have already been realized experimentally [3,8].

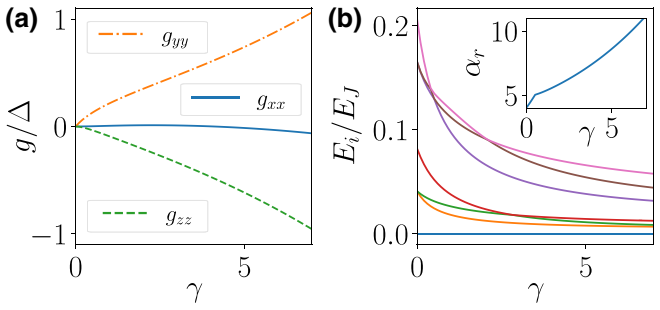

FIG. 3. (a) Coupling strength in gap units and (b) low-energy spectrum for two equal 3JJQs capacitively coupled, both having $\alpha = 0.65$ and ratio $E_J/E_C = 50$, as a function of the ratio $\gamma = C_g/C$ between the shared capacitance and the qubit's large junction capacitance. The E_J, E_C are the Josephson and charging energies of the large junction qubit. The inset of (b) shows the relative anharmonicity of each qubit approximated from the full spectrum as $\alpha_r = (E_3 - E_0 - \Delta)/\Delta$.

We interpret these results using the perturbation theory in Eq. (3), with processes $\mathcal{M}_1$, $\mathcal{M}_2$, and $\mathcal{M}_3$, sketched in Figs. 4(a)–4(c). The horizontal lines denote qubit (solid) and excited states (dashed). These are connected by interactions (wiggly lines), which can be qubit terms P_0VP_0 (blue) or connect to excitations $P_0V(\mathbb{1} - P_0)$ and $(\mathbb{1} - P_0)VP_0$ (red). To first order, the capacitor produces YY terms in the qubit space. To second order, the operator V_c enables virtual transitions where both circuits momentarily excite, acquiring an energy of approximately $2 \times \hbar\omega_q$. Despite the large energy difference, these processes are assisted by matrix elements in V_c that grow as ω_q, and cannot be neglected. We estimate the second-order term $H_{qq}^{(2)} = g_{qq}^{(2)}\sigma_1^z\sigma_2^z$ with a coupling that scales as

$$g_{qq}^{(2)} \sim \left(\frac{C_q}{\overline{C}_{\text{OD}}}\right)^2 \frac{(\Delta_e - \Delta)^2}{\hbar\omega_q}, \tag{6}$$

where Δ_e is the approximate splitting between excited states due to tunneling [see the Appendix C and Fig. 1(a)]. Finally, we can also deduce that third-order terms create an XX coupling. This coupling becomes dominant when the renormalization of the qubit's capacitance enables phase-slip transitions between the qubit's unit cells—as opposed to the tunneling between current states enabled by Δ. However, this mechanism leads to an enhancement of charge noise [1,42]. We can stay far from this regime by

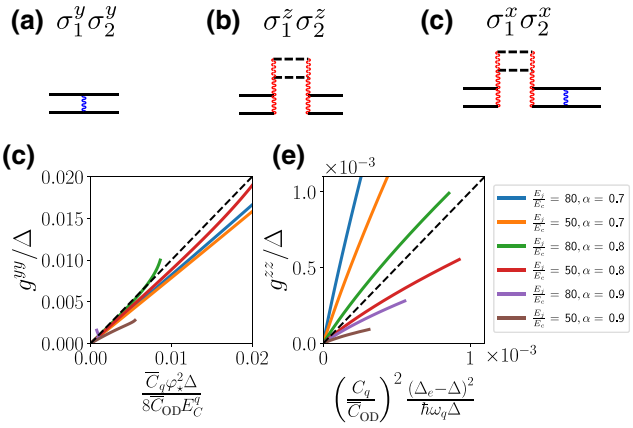

FIG. 4. Diagrams for (a) first-, (b) second-, and (c) third-order corrections to the capacitive coupling of two 3JJQs. Qubit and excited states are represented by solid and dashed lines, respectively. Wiggle lines are qubit interactions, which can be diagonal (shorter blue line) and off diagonal (longer red) in the qubit subspace. First-order corrections are the projection of charge-charge operators to the qubit subspace. It gives a YY type of coupling. Second-order corrections produce a ZZ type of coupling. We only show one of the possible diagrams for third-order corrections. It can be seen to give XX coupling using the lower-order diagrams. Data collapse of the (d) first- and (e) second-order corrections for several qubit design parameters. In the first case, we only show data for which higher corrections are negligible.

limiting $\gamma \sim O(1)$ and choosing $\alpha < 0.9$, away from the single qubit phase-slip regime [1]. This way we can still recover an XX interaction by coupling the qubits inductively, which in combination with YY and ZZ interactions gives a fully nonstoquastic spin model.

As in the resonator case, we compare our predictions (5) and (6) to the numerically exact couplings for different qubit designs. Figure 3(d) shows how the g^{yy} coupling collapses to the theoretical prediction (5) only for small enough couplings $g/\Delta < 0.05$. Similarly, Fig. 3(e) shows that g^{zz} follows the expected scaling, up to factors $\mathcal{O}(1)$. This is a reasonable agreement, taking into account that we have taken the two excited states deep enough inside of the potential wells, so that their dynamic is mainly due to the tunneling Δ_e; see Fig. 1(b) and Appendix C. In fact, we can see that the data collapse is better for $\alpha \geq 0.8$, which is indeed the regime of deep potential wells. Perturbation theory thus captures the overall dependency of the couplings on the qubit's parameters, but fails to estimate the nonperturbative corrections that account for the full interaction. This contrasts with the qubit-resonator model, and highlights the relevance of qubit-qubit interactions mediated by excited states.

VII. CONCLUSIONS

We have presented a nonperturbative study of capacitive interactions between a flux qubit and other circuits. This study reveals that the flux qubit charge operator is the sum of two dipole moments: one connecting qubit states and one enabling transitions to higher-energy excitations. The first term describes the coupling between a qubit and a resonator and supports ultrastrong qubit-photon interactions along directions orthogonal to those created by inductive terms. The second term combines with the first one to enable a rich family of nonstoquastic qubit-qubit couplings, including YY, ZZ, and XX interactions.

The capacitive interactions combined with inductive ultrastrong qubit-photon interactions [17,18,22,23] open regimes in light-matter and light-mediated interactions, such as the ultrastrong coupling limit of the Jaynes-Cummings model [53], regimes of the spin-boson model [22] with two transverse couplings, and models of coherent and dissipative interactions mediated by photon exchange, beyond those in Ref. [54].

Regarding quantum simulation, our study confirms the idea that flux qubits exhibit rich families of nonstoquastic interactions. These may appear combined, as in the two-qubit model, or they may be pure YY interactions, if we use resonators to mediate the coupling [27,55]. From a fundamental point of view, it would be interesting to explore the long-range interactions at the hardware level, without embeddings [56]. Indeed, capacitively coupled flux qubits in two-dimensional geometries support YY interactions that only decay logarithmically up to a length $\xi = \sqrt{C_g/C_q}$ and then exponentially fast [57]. As in classical spin glasses, such long-range interactions will produce hard to solve quantum models [58–62].

Finally, recent works [63,64] suggest that the *ground-state properties* of many superconducting circuits, including capacitively coupled flux qubits, could be efficiently simulable in the semiclassical charge-flux representation. Our work opens a rigorous avenue to study these circuits and their effective models in a nonperturbative fashion. This will help us understand whether the ground states of circuits are in some sense trivial—e.g., low-energy states are classical spin configurations—or whether the energy scales and types of interactions reveal other kinds of obstructions, different from the sign problem, that prevent the classical simulation of the device.

ACKNOWLEDGMENTS

This work is supported by the European Commission FET-Open project AVaQus GA 899561 and CSIC Quantum Technologies Platform PTI-001. Financial support by Fundación General CISC (Programa Comfuturo) is acknowledged. The numerical computations have been performed in the cluster Trueno of the CSIC.

APPENDIX A: HAMILTONIAN OF TWO FLUX QUBITS COUPLED VIA A CAPACITOR

We derive the Hamiltonian for a system of two flux qubits coupled via a capacitor. We assume two identical qubits, with qubit capacitance C_q, which are coupled by a capacitor C_g as in Fig. 1 of the main text. The Lagrangian is written in terms of the capacitance matrix as

$$\mathcal{L} = \frac{1}{2}\dot{\vec{\phi}}\mathcal{C}\dot{\vec{\phi}} - \sum_{i=1,2}\mathcal{U}_i \tag{A1}$$

with the vector of fluxes of each qubit $\vec{\phi} = (\phi_1, \phi_2)$ and the capacitance matrix

$$\mathcal{C} = \begin{bmatrix} C_q + C_g & -C_g \\ -C_g & C_q + C_g \end{bmatrix}. \tag{A2}$$

The Hamiltonian $H = \sum_{i=1,2} q_i\dot{\phi}_i - \mathcal{L}$ can be written using the flux and its conjugate charge:

$$H = \sum_{i=1,2}\frac{q_i^2}{2\overline{C}_q} + \mathcal{U}(\phi_i) + \frac{q_1 q_2}{\overline{C}_{\mathrm{OD}}}. \tag{A3}$$

The inverse of capacitance matrix $\mathcal{C}^{-1}$ is used to obtain $1/\overline{C}_q = (\mathcal{C}^{-1})_{11} = (\mathcal{C}^{-1})_{22}$ and $1/\overline{C}_{\mathrm{OD}} = (\mathcal{C}^{-1})_{12} = (\mathcal{C}^{-1})_{21}$.

We can obtain the following expressions for the capacitances involved in Eq. (A3):

$$\frac{1}{\overline{C}_q} = \frac{1}{C_q}\frac{C_q + C_g}{2C_g + C_q}, \tag{A4}$$

$$\frac{1}{\overline{C}_{\rm OD}} = \frac{1}{C_q}\frac{C_g}{2C_g + C_q}. \tag{A5}$$

Taking into account the fact that the renormalized qubit matrix is $1/\overline{C}_q = 1/C_q - 1/\overline{C}_{\rm OD}$, we express the Hamiltonian as a sum of the noncoupled Hamiltonian H_0 plus a perturbation V, as in Eq. (2) of the main text:

$$H = H^{(0)} + \epsilon V, \tag{A6}$$

$$H^{(0)} = \sum_{i=1,2} \frac{q_i^2}{2C_q} + \mathcal{U}(\phi_i), \tag{A7}$$

$$V = \frac{q_1 q_2}{C_q} - \sum_{i=1,2} \frac{q_i^2}{2C_q}. \tag{A8}$$

Here $\epsilon = C_q/\overline{C}_{\rm OD}$. The second term in the previous Hamiltonian is a perturbation to the noncoupled system when $\epsilon \ll 1$. The Hamiltonian for the general case, Eq. (2) with asymmetric capacitances C_1, C_2, can be obtained from the inverse of the capacitance matrix $1/\overline{C}_1 = 1/C_1 - C_2/(\overline{C}_{\rm OD}C_1)$ and $1/\overline{C}_2 = 1/C_2 - C_1/(\overline{C}_{\rm OD}C_2)$.

APPENDIX B: PERTURBATION THEORY FOR THE CAPACITIVE COUPLING OF TWO FLUX QUBITS

We use the Schrieffer-Wolff transformation [45] and expand the effective Hamiltonian as a series in ascending powers of the small parameter ϵ, as in Eq. (3) of the main text. The perturbation series up to third order can be expressed as

$$H_{\rm eff} = H^{(0)} + \epsilon\mathcal{M}_1 + \epsilon^2\mathcal{M}_2 + \epsilon^3\mathcal{M}_3 \tag{B1}$$

with matrices

$$\mathcal{M}_1 = P_0 V P_0, \tag{B2}$$

$$\mathcal{M}_2 = \tfrac{1}{2} P_0 \hat{S}(V_{\rm OD}) P_0, \tag{B3}$$

$$\mathcal{M}_3 = \tfrac{1}{2} P_0 \hat{V}_{\rm OD} \mathcal{L} \hat{V}_d(S) P_0, \tag{B4}$$

where the adjoint representation is $\hat{Y}(X) = [Y, X]$ and the operators P_0, Q_0 project onto the qubit and excited subspaces of the unperturbed system. The notation $O_{\rm OD}$ is used for the nondiagonal part of an operator, $O_{\rm OD} = P_0 O Q_0 + Q_0 O P_0$, and $S = \mathcal{L}(V_{\rm OD})$ with $\mathcal{L}(O) = \sum_{ij} (O_{\rm OD})_{ij}/E_{ij} |j\rangle\langle i|$ (matrix elements are denoted by $O_{ij} = \langle i|O|j\rangle$ and energy differences by $E_{ij} = E_i - E_j$).

We now give the explicit forms of the matrices involved in the computation of the effective Hamiltonian up to third order. We do so by employing Latin and Greek letters to denote unperturbed qubit and excited states, respectively. We have

$$\mathcal{M}_1 = \sum_{i,j} V_{ij} |j\rangle\langle i|, \tag{B5}$$

$$\mathcal{M}_2 = \frac{1}{2} \sum_{i,j,\alpha} \frac{V_{i\alpha} V_{\alpha j}}{E_{i\alpha}} (|j\rangle\langle i| + |i\rangle\langle j|), \tag{B6}$$

$$\mathcal{M}_3 = \frac{1}{2}\left(\sum_{\alpha,j,\beta,k} \frac{V_{j\alpha} V_{\alpha\beta} V_{\beta k}}{E_{\alpha j} E_{\beta j}} - \sum_{\alpha,i,j,k} \frac{V_{ji} V_{i\alpha} V_{\alpha k}}{E_{\alpha i} E_{\alpha j}} \right) \times (|k\rangle\langle j| + |j\rangle\langle k|), \tag{B7}$$

where the braket of the interactions in the qubit subspace $V_{ij} = \langle i|V|j\rangle$, on the excited one $V_{\alpha\beta} = \langle\alpha|V|\beta\rangle$, and the off diagonal between qubit and excited states $V_{\alpha i} = \langle\alpha|V|i\rangle$.

As discussed in the main text, the first-order corrections, Eq. (B5), are given by the projection of the perturbation to the qubit subspace. They produce a renormalization of the gap mass and a coupling of YY type. The higher-order corrections that couple the qubits involve operators that move the state of the superconducting circuit from a qubit to excited state. We analyze in the following those corrections.

APPENDIX C: SECOND- AND THIRD-ORDER CORRECTIONS TO QUBIT-QUBIT COUPLING

We focus now on the second-order correction for two 3JJQs coupled via a capacitor. We do not analyze contributions that renormalize each qubit gap, only contributions that couple the two-qubit system. The relevant diagram is shown in Fig. 3(b) of the main text, where the qubits visit high-energy states due to the off-diagonal part of the interaction. We need to make strong simplifications on the qubit spectrum, as we explain in what follows, in order to analytically treat second-order corrections. Each qubit is approximated by the first fourth eigenstate of the uncoupled superconducting circuit. We use the notation $|\pm_g\rangle = (|L_e\rangle \pm |R_e\rangle)$ for the qubit eigenstates and $|\pm_e\rangle = (|L_e\rangle \pm |R_e\rangle)$ for second and third excited states, where $|L_g\rangle$ and $|L_e\rangle$ are the ground and first excited states inside the left well of the potential, with similar notation ($|R_g\rangle$ and $|R_e\rangle$) for the right well; see Fig. 1(b) of the main text for a picture of the spectrum.

The unperturbed projected Hamiltonian onto the subspace expanded by the first four states of each qubit is

$$H^{(0)} = \sum_{i=1,2} \frac{\Delta}{2} P_{0i}^\dagger \sigma_i^z P_{0i} + \sum_{i=1,2} Q_{0i}^\dagger \left(\hbar\omega_q + \frac{\Delta_e}{2}\sigma_i^z \right) Q_{0i}, \tag{C1}$$

where P_{0i} and Q_{0i} project onto the unperturbed low and excited subspaces of qubit i, respectively. We have extended the domain of Pauli matrices so that they act on ground $\sigma_i^z|\pm_g\rangle = \pm|\pm_g\rangle$ and excited $\sigma_i^z|\pm_e\rangle = \pm|\pm_e\rangle$ states. We need to compute the nondiagonal energy between the low-energy and high-energy sectors to obtain the second-order term. We recall that, in the case treated here, $V_{\rm OD} = P_0VQ_0 + Q_0VP_0$, so that we can approximate the off-diagonal elements of the interaction as

$$V_{i_g,\alpha_e} = \langle i_g|\frac{q_1q_2}{C_q}|\alpha_e\rangle \approx \hbar\omega_q\delta_{i\alpha}, \tag{C2}$$

where $i,\alpha = 1,2,3,4$. The low-energy sector of the coupled system is $|1_g\rangle = |+_g,+_g\rangle$, $|2_g\rangle = |+_g,-_g\rangle$, $|3_g\rangle = |-_g,+_g\rangle$, and $|4_g\rangle = |-_g,-_g\rangle$. Similarly, for the excited states, we have $|1_e\rangle = |+_e,+_e\rangle$, $|2_e\rangle = |+_e,-_e\rangle,\ldots$. The effective harmonic frequency of each of the single-qubit potential wells is ω_q; see Fig. 1(b) of the main text. We do not consider a matrix process that takes only one qubit outside of the low-energy subspace and brings it back. Those processes have an amplitude that scales as $\sqrt{\hbar\omega_q\Delta}$, which is much smaller than that which takes the two qubits outside of the qubit subspace in Eq. (C2) (we are in the anharmonic limit $\Delta \ll \hbar\omega_q$). We then approximate the second-order corrections as

$$\frac{1}{(\hbar\omega_q)^2}\mathcal{M}_2 = \frac{|+_g+_g\rangle\langle+_g+_g|}{2\hbar\omega_q + (\Delta_e - \Delta)} + \frac{|-_g-_g\rangle\langle-_g-_g|}{2\hbar\omega_q - (\Delta_e - \Delta)} + \frac{|-_g+_g\rangle\langle-_g+_g| + |+_g-_g\rangle\langle+_g-_g|}{2\hbar\omega_q}. \tag{C3}$$

Expanding the denominator up to second order in $\Delta_e - \Delta$ and using the identity $|\pm\rangle\langle\pm| = (1 \pm \sigma^z)/2$, we find that

$$H^{(2)} = g_{qq}^{(2)}\sigma_1^z\sigma_2^z, \tag{C4}$$

$$g_{qq}^{(2)} \sim \epsilon^2\frac{(\Delta_e - \Delta)^2}{\hbar\omega_q}. \tag{C5}$$

We then find a $\sigma_1^z\sigma_2^z$ with an amplitude that, up to a multiplicative constant, scales approximately as predicted in the previous formula. The multiplicative factor that arises from our analysis is not reliable. The reason is that, due to the departure of the qubit potential wells from simple harmonic oscillators, we cannot fix the exact value of the coupling in Eq. (C2) or the energy difference between the low- and high-energy subspaces. However, we know that those two quantities should scale with the approximate effective well frequency $\hbar\omega_q$, which is enough to find the scaling form in Eq. (C2).

In the case of two 3JJQs, we can express the previous formula using the ratio between the large Josephson junction and coupling capacitances $\gamma = C_g/C$, instead of the parameter in the perturbative expansion via $\epsilon = C_q/\overline{C}_{\rm OD} = \gamma/[2(1+2\alpha+\gamma)]$. The second-order corrections are then

$$g_{qq}^{(2)} \sim \frac{\gamma^2}{\hbar\omega_q}\left(\frac{\Delta_e - \Delta}{1+2\alpha+2\gamma}\right)^2. \tag{C6}$$

This is the formula that is used to plot the results in Fig. 4 of the main text. We note that our scaling only works for very deep potential wells as we have assumed that the two excited states in each well are mainly connected by tunneling Δ_e. This is not the case for shallow potential wells where the overlap of those states is large. Thus, we expect that Eq. (C5) describes the scaling only when α is large enough, $\alpha \leq 0.8$, a regime in which the potential well separating the two persistent current states is indeed quite deep.

Using similar approximations as before, we find that third-order corrections produce a coupling of the type $\sigma_1^x\sigma_2^x$. To this end, we analyze the third-order correction corresponding to the second term inside the parentheses on the right-hand side of Eq. (B7). These corrections can be approximated as

$$g_{qq}^{(3)} \approx \sum_{\alpha,i,j,k}\frac{V_{ji}V_{i\alpha}V_{\alpha k}}{E_{\alpha i}E_{\alpha j}} = \frac{\mathcal{M}_1}{\hbar\omega_q}\mathcal{M}_2. \tag{C7}$$

Taking into account the shape of the first two corrections, this term would give a contribution to coupling $\sigma_1^x\sigma_2^x$ as explained in Fig. 3. Although there are other corrections at third order, this simple analysis shows that the XX coupling will first appear at third order, which is consistent with what we see in the numerical data from Fig. 3 of the main text, where g_{xx} depends on ϵ^3 at small ϵ.

[1] T. P. Orlando, J. E. Mooij, Lin Tian, Caspar H. Van Der Wal, L. S. Levitov, Seth Lloyd, and J. J. Mazo, Superconducting persistent-current qubit, Phys. Rev. B **60**, 15398 (1999).

[2] J. E. Mooij, T. P. Orlando, L. Levitov, Lin Tian, Caspar H. Van der Wal, and Seth Lloyd, Josephson persistent-current qubit, Science **285**, 1036 (1999).

[3] I. Chiorescu, Y. Nakamura, C. J. P. Ma Harmans, and J. E. Mooij, Coherent quantum dynamics of a superconducting flux qubit, Science **299**, 1869 (2003).

[4] J. T. Peltonen, P. C. J. J. Coumou, Z. H. Peng, T. M. Klapwijk, J. S. Tsai, and O. V. Astafiev, Hybrid rf squid qubit based on high kinetic inductance, Sci. Rep. **8**, 1 (2018).

[5] J. Q. You, Xuedong Hu, S. Ashhab, and Franco Nori, Low-decoherence flux qubit, Phys. Rev. B **75**, 140515 (2007).

[6] Jonas Bylander, Simon Gustavsson, Fei Yan, Fumiki Yoshihara, Khalil Harrabi, George Fitch, David G. Cory, Yasunobu Nakamura, Jaw-Shen Tsai, and William D. Oliver, Noise spectroscopy through dynamical decoupling with a superconducting flux qubit, Nat. Phys. **7**, 565 (2011).

[7] Michael Stern, Gianluigi Catelani, Yuimaru Kubo, Cecile Grezes, Audrey Bienfait, Denis Vion, Daniel Esteve, and Patrice Bertet, Flux Qubits with Long Coherence Times for Hybrid Quantum Circuits, Phys. Rev. Lett. **113**, 123601 (2014).

[8] Fei Yan, Simon Gustavsson, Archana Kamal, Jeffrey Birenbaum, Adam P. Sears, David Hover, Ted J. Gudmundsen, Danna Rosenberg, Gabriel Samach, Steven Weber, *et al.*, The flux qubit revisited to enhance coherence and reproducibility, Nat. Commun. **7**, 1 (2016).

[9] Jochen Braumüller, Leon Ding, Antti P. Vepsäläinen, Youngkyu Sung, Morten Kjaergaard, Tim Menke, Roni Winik, David Kim, Bethany M. Niedzielski, Alexander Melville, *et al.*, Characterizing and Optimizing Qubit Coherence Based on Squid Geometry, Phys. Rev. Appl. **13**, 054079 (2020).

[10] Yu-Xi Liu, L. F. Wei, J. S. Tsai, and Franco Nori, Controllable Coupling Between Flux Qubits, Phys. Rev. Lett. **96**, 067003 (2006).

[11] Shiro Saito, Todd Tilma, Simon J. Devitt, Kae Nemoto, and Kouich Semba, Experimentally realizable controlled not gate in a flux qubit/resonator system, Phys. Rev. B **80**, 224509 (2009).

[12] Tadashi Kadowaki and Hidetoshi Nishimori, Quantum annealing in the transverse Ising model, Phys. Rev. E **58**, 5355 (1998).

[13] P. I. Bunyk, Emile M. Hoskinson, Mark W. Johnson, Elena Tolkacheva, Fabio Altomare, Andrew J. Berkley, Richard Harris, Jeremy P. Hilton, Trevor Lanting, Anthony J. Przybysz, *et al.*, Architectural considerations in the design of a superconducting quantum annealing processor, IEEE Trans. Appl. Supercond. **24**, 1 (2014).

[14] Sergio Boixo, Troels F. Rønnow, Sergei V. Isakov, Zhihui Wang, David Wecker, Daniel A. Lidar, John M. Martinis, and Matthias Troyer, Evidence for quantum annealing with more than one hundred qubits, Nat. Phys. **10**, 218 (2014).

[15] Steven J. Weber, Gabriel O. Samach, David Hover, Simon Gustavsson, David K. Kim, Alexander Melville, Danna Rosenberg, Adam P. Sears, Fei Yan, Jonilyn L. Yoder, William D. Oliver, and Andrew J. Kerman, Coherent Coupled Qubits for Quantum Annealing, Phys. Rev. Appl. **8**, 014004 (2017).

[16] Philipp Hauke, Helmut G. Katzgraber, Wolfgang Lechner, Hidetoshi Nishimori, and William D. Oliver, Perspectives of quantum annealing: Methods and implementations, Rep. Prog. Phys. **83**, 054401 (2020).

[17] Thomas Niemczyk, F. Deppe, H. Huebl, E. P. Menzel, F. Hocke, M. J. Schwarz, J. J. Garcia-Ripoll, D. Zueco, T. Hümmer, E. Solano, *et al.*, Circuit quantum electrodynamics in the ultrastrong-coupling regime, Nat. Phys. **6**, 772 (2010).

[18] Pol Forn-Díaz, Jürgen Lisenfeld, David Marcos, Juan José Garcia-Ripoll, Enrique Solano, C. J. P. M. Harmans, and J. E. Mooij, Observation of the Bloch-Siegert Shift in a Qubit-Oscillator System in the Ultrastrong Coupling Regime, Phys. Rev. Lett. **105**, 237001 (2010).

[19] Borja Peropadre, Pol Forn-Díaz, Enrique Solano, and Juan José García-Ripoll, Switchable Ultrastrong Coupling in Circuit Qed, Phys. Rev. Lett. **105**, 023601 (2010).

[20] Kosuke Kakuyanagi, Yuichiro Matsuzaki, Corentin Déprez, Hiraku Toida, Kouichi Semba, Hiroshi Yamaguchi, William J. Munro, and Shiro Saito, Observation of Collective Coupling Between an Engineered Ensemble of Macroscopic Artificial Atoms and a Superconducting Resonator, Phys. Rev. Lett. **117**, 210503 (2016).

[21] M. Pino, A. M. Tsvelik, and L. B. Ioffe, Unpaired Majorana Modes in Josephson-Junction Arrays with Gapless Bulk Excitations, Phys. Rev. Lett. **115**, 197001 (2015).

[22] P. Forn-Díaz, J. José García-Ripoll, Borja Peropadre, J.-L. Orgiazzi, M. A. Yurtalan, R. Belyansky, Christopher M. Wilson, and A. Lupascu, Ultrastrong coupling of a single artificial atom to an electromagnetic continuum in the nonperturbative regime, Nat. Phys. **13**, 39 (2017).

[23] Fumiki Yoshihara, Tomoko Fuse, Sahel Ashhab, Kosuke Kakuyanagi, Shiro Saito, and Kouichi Semba, Superconducting qubit–oscillator circuit beyond the ultrastrong-coupling regime, Nat. Phys. **13**, 44 (2017).

[24] Daniele De Bernardis, Philipp Pilar, Tuomas Jaako, Simone De Liberato, and Peter Rabl, Breakdown of gauge invariance in ultrastrong-coupling cavity qed, Phys. Rev. A **98**, 053819 (2018).

[25] Xiaobo Zhu, Shiro Saito, Alexander Kemp, Kosuke Kakuyanagi, Shin-Ichi Karimoto, Hayato Nakano, William J. Munro, Yasuhiro Tokura, Mark S. Everitt, Kae Nemoto, *et al.*, Coherent coupling of a superconducting flux qubit to an electron spin ensemble in diamond, Nature **478**, 221 (2011).

[26] M. Pino and J. J. García-Ripoll, Mediator-assisted cooling in quantum annealing, Phys. Rev. A **101**, 032324 (2020).

[27] Manuel Pino and Juan José García-Ripoll, Quantum annealing in spin-boson model: From a perturbative to an ultrastrong mediated coupling, New J. Phys. **20**, 113027 (2018).

[28] Sergey Bravyi, David P. Divincenzo, Roberto Oliveira, and Barbara M. Terhal, The complexity of stoquastic local hamiltonian problems, Quantum Inf. Comput. **8**, 361 (2008).

[29] Yuki Susa, Johann F. Jadebeck, and Hidetoshi Nishimori, Relation between quantum fluctuations and the performance enhancement of quantum annealing in a nonstoquastic hamiltonian, Phys. Rev. A **95**, 042321 (2017).

[30] Tameem Albash, Role of nonstoquastic catalysts in quantum adiabatic optimization, Phys. Rev. A **99**, 042334 (2019).

[31] Layla Hormozi, Ethan W. Brown, Giuseppe Carleo, and Matthias Troyer, Nonstoquastic Hamiltonians and quantum annealing of an Ising spin glass, Phys. Rev. B **95**, 184416 (2017).

[32] Isil Ozfidan, Chunqing Deng, A. Y. Smirnov, T. Lanting, R. Harris, L. Swenson, J. Whittaker, F. Altomare, M. Babcock, C. Baron, *et al.*, Demonstration of a Nonstoquastic Hamiltonian in Coupled Superconducting Flux Qubits, Phys. Rev. Appl. **13**, 034037 (2020).

[33] Tameem Albash and Daniel A. Lidar, Adiabatic quantum computation, Rev. Mod. Phys. **90**, 015002 (2018).

[34] Alexei Yu Kitaev, Alexander Shen, Mikhail N. Vyalyi, and Mikhail N. Vyalyi, *Classical and Quantum Computation* (American Mathematical Soc., 2002), Vol. 47

[35] Julia Kempe and Oded Regev, 3-local Hamiltonian is QMA-complete, preprint ArXiv:quant-ph/0302079 (2003).

[36] Julia Kempe, Alexei Kitaev, and Oded Regev, The complexity of the local hamiltonian problem, SIAM J. Comput. **35**, 1070 (2006).

[37] Roberto Oliveira and Barbara M. Terhal, The complexity of quantum spin systems on a two-dimensional square lattice, preprint ArXiv:quant-ph/0504050 (2005).
[38] Andrew J. Kerman, Superconducting qubit circuit emulation of a vector spin-1/2, New J. Phys. **21**, 073030 (2019).
[39] Jonathan R. Friedman and Dmitri V. Averin, Aharonov-Casher-Effect Suppression of Macroscopic Tunneling of Magnetic Flux, Phys. Rev. Lett. **88**, 050403 (2002).
[40] M. T. Bell, Wenyuan Zhang, L. B. Ioffe, and M. E. Gershenson, Spectroscopic Evidence of the Aharonov-Casher Effect in a Cooper Pair Box, Phys. Rev. Lett. **116**, 107002 (2016).
[41] Konstantin Kalashnikov, Wen Ting Hsieh, Wenyuan Zhang, Wen-Sen Lu, Plamen Kamenov, Agustin Di Paolo, Alexandre Blais, Michael E. Gershenson, and Matthew Bell, Bifluxon: Fluxon-parity-protected superconducting qubit, PRX Quantum **1**, 010307 (2020).
[42] Luca Chirolli and Guido Burkard, Full control of qubit rotations in a voltage-biased superconducting flux qubit, Phys. Rev. B **74**, 174510 (2006).
[43] Takahiko Satoh, Yuichiro Matsuzaki, Kosuke Kakuyanagi, Koichi Semba, Hiroshi Yamaguchi, and Shiro Saito, Ising interaction between capacitively-coupled superconducting flux qubits, Preprint ArXiv:1501.07739 (2015).
[44] Gioele Consani and Paul A. Warburton, Effective Hamiltonians for interacting superconducting qubits: Local basis reduction and the Schrieffer–Wolff transformation, New J. Phys. **22**, 053040 (2020).
[45] Sergey Bravyi, David P. DiVincenzo, and Daniel Loss, Schrieffer–Wolff transformation for quantum many-body systems, Ann. Phys. (N. Y.) **326**, 2793 (2011).
[46] Marí Hita-Pérez, Gabriel Jaumà, Manuel Pino, and Juan José Garcí-Ripoll, Three-Josephson junctions flux qubit couplings, Appl. Phys. Lett. **119**, 222601 (2021).
[47] Vladimir E. Manucharyan, Jens Koch, Leonid I. Glazman, and Michel H. Devoret, Fluxonium: Single cooper-pair circuit free of charge offsets, Science **326**, 113 (2009).
[48] Uri Vool, Ioan M. Pop, Katrina Sliwa, Baleegh Abdo, Chen Wang, Teresa Brecht, Yvonne Y. Gao, Shyam Shankar, Michael Hatridge, Gianluigi Catelani, *et al.*, Non-Poissonian Quantum Jumps of a Fluxonium Qubit Due to Quasiparticle Excitations, Phys. Rev. Lett. **113**, 247001 (2014).
[49] Kunihiro Inomata, Tsuyoshi Yamamoto, P.-M. Billangeon, Y. Nakamura, and J. S. Tsai, Large dispersive shift of cavity resonance induced by a superconducting flux qubit in the straddling regime, Phys. Rev. B **86**, 140508 (2012).
[50] T. Yamamoto, K. Inomata, K. Koshino, P. M. Billangeon, Y. Nakamura, and J. S. Tsai, Superconducting flux qubit capacitively coupled to an LC resonator, New J. Phys. **16**, 015017 (2014).
[51] Matilda Peruzzo, Farid Hassani, Gregory Szep, Andrea Trioni, Elena Redchenko, Martin Žemlička, and Johannes Fink, Geometric superinductance qubits: Controlling phase delocalization across a single Josephson junction, PRX Quantum **2**, 040341 (2021).
[52] L. S. Levitov, T. P. Orlando, J. B. Majer, and J. E. Mooij, Quantum spin chains and Majorana states in arrays of coupled qubits, Preprint ArXiv:cond-mat/0108266 (2001).
[53] Jin-Feng Huang, Jie-Qiao Liao, and Le-Man Kuang, Ultrastrong Jaynes-Cummings model, Phys. Rev. A **101**, 043835 (2020).
[54] A. Gonzalez-Tudela, D. Martin-Cano, E. Moreno, L. Martin-Moreno, C. Tejedor, and F. J. Garcia-Vidal, Entanglement of Two Qubits Mediated by One-Dimensional Plasmonic Waveguides, Phys. Rev. Lett. **106**, 020501 (2011).
[55] Andreas Kurcz, Alejandro Bermudez, and Juan José Garcia-Ripoll, Hybrid Quantum Magnetism in Circuit Qed: From Spin-Photon Waves to Many-Body Spectroscopy, Phys. Rev. Lett. **112**, 180405 (2014).
[56] Davide Venturelli, Salvatore Mandrà, Sergey Knysh, Bryan O'Gorman, Rupak Biswas, and Vadim Smelyanskiy, Quantum Optimization of Fully Connected Spin Glasses, Phys. Rev. X **5**, 031040 (2015).
[57] M. Ortuño, A. M. Somoza, V. M. Vinokur, and T. I. Baturina, Electronic transport in two-dimensional high dielectric constant nanosystems, Sci. Rep. **5**, 1 (2015).
[58] L. A. Fernandez, E. Marinari, V. Martin-Mayor, G. Parisi, and J. J. Ruiz-Lorenzo, Out-of-equilibrium 2D Ising spin glass: Almost, but not quite, a free-field theory, J. Stat. Mech.: Theory Exp. **2018**, 103301 (2018).
[59] L. A. Fernandez, E. Marinari, V. Martin-Mayor, G. Parisi, and J. J. Ruiz-Lorenzo, An experiment-oriented analysis of 2D spin-glass dynamics: A twelve time-decades scaling study, J. Phys. A: Math. Theor. **52**, 224002 (2019).
[60] Jeffrey Marshall, Victor Martin-Mayor, and Itay Hen, Practical engineering of hard spin-glass instances, Phys. Rev. A **94**, 012320 (2016).
[61] M. Pino, A. M. Somoza, and M. Ortuño, Quantum coulomb gap in low dimensions, Phys. Rev. B **86**, 094202 (2012).
[62] M. Pino, Scaling up the Anderson transition in random-regular graphs, Phys. Rev. Res. **2**, 042031 (2020).
[63] Alessandro Ciani and Barbara M. Terhal, Stoquasticity in circuit qed, Phys. Rev. A **103**, 042401 (2021).
[64] Tom Halverson, Lalit Gupta, Moshe Goldstein, and Itay Hen, Efficient simulation of so-called non-stoquastic superconducting flux circuits, ArXiv:2011.03831 (2020).